JOURNAL OF CATALYSIS 76, 450–465 (1982)

Simultaneous Measurement of CO Oxidation Rate and Surface Coverage on Pt/Al_2O_3 Using Infrared Spectroscopy: Rate Hysteresis and CO Island Formation[1]

DAVID M. HAALAND* AND FRANK L. WILLIAMS†

*Sandia National Laboratories,[2] Albuquerque, New Mexico 87185, and †Chemical & Nuclear Engineering Department, University of New Mexico, Albuquerque, New Mexico 87131

Received June 26, 1981; revised February 23, 1982

The catalytic oxidation of CO on a commercial Pt/Al_2O_3 catalyst has been studied at a total pressure of one atmosphere using Fourier transform infrared spectroscopy. Simultaneous measurements of steady-state reaction rates and CO surface coverages were obtained at temperatures between 460 and 520 K. During oxidation, the frequency of the infrared absorption peak of linear-bonded CO is invariant at 2081 cm^{-1} at 520 K over nearly a 100-fold change in CO surface coverage. This peak position is within 1 cm^{-1} of that found for saturation coverage in the presence of pure CO at one atmosphere. In contrast, under nonreactive desorption, large shifts in frequency are found as the CO surface coverage changes. The ratio of the intensities of the absorption bands due to both linear and bridge-bonded CO was constant during oxidation. These observations are interpreted as resulting from the formation of islands of CO during the oxidation reaction. Hysteresis in both CO reaction probability and CO surface coverage are found which are inversely related. Thus CO blocks active sites on the Pt for the reaction. The width and shape of the hysteresis loops as a function of temperature are qualitatively understood in terms of the rate of CO desorption from the Pt surface. At very high surface coverages, changes in the reaction probability are not accompanied by changes in adsorbed CO. This may be due either to the formation of surface species, unobserved in ir, which block the reaction or to the presence of a small number of very reactive Pt sites which are blocked with only a very small change in CO surface coverage.

INTRODUCTION

The catalytic oxidation of carbon monoxide has been studied extensively because of its practical importance and the relative simplicity of the reaction. Much of the effort expended in trying to elucidate the sequence of elementary steps in CO oxidation has been directed at polycrystalline and single crystal metal surfaces at low pressures ($\leq 10^{-2}$ Pa). The literature related to surface studies of CO adsorption and low pressure CO oxidation on metal surfaces has been recently reviewed by Engel and Ertl (*1*). Recent analyses on a wide variety of metal surfaces at low pressure (*2–12*) strongly support the Langmuir–Hinshelwood mechanism (CO_{ad} reacting with O_{ad}) over the alternate Eley–Rideal mechanism (CO in the gas phase or in a weakly bound precursor state reacting with adsorbed oxygen). However, the commonly employed assumption that the adsorbed reactants are in equilibrium with the gas phase does not appear to be generally valid for CO oxidation on Pt. For example, Herz and Marin (*13*) invoke rate-limiting adsorption kinetics to fit CO oxidation rate data on Pt/Al_2O_3 at atmospheric pressure. Creighton *et al.* (*14*) have reached the same conclusions for CO oxidation at low pressures on Pt foils. There is also a growing body of experimental data which suggests that domains or islands of the reactants form during the low pressure oxidation of CO (*3–5, 9, 10, 15, 16*). Engel and Ertl (*1*) provide arguments that, below the temperature for which the reaction reaches its maximum rate, the catalytic reaction of CO is only affected by the ratio of partial pressures of reactants and not the

[1] This work was supported by the United States Department of Energy (DOE) under Contract DE-AC04-76-DP00789.

[2] A DOE facility.

0021-9517/82/080450-16$02.00/0

total pressure, i.e., $r_{CO} = kP_{O_2}/P_{CO}$. These authors point out that knowledge acquired about this reaction at low pressure may be able to leep the "pressure gap" and thereby be applicable at high pressures. The series of experiments at low pressure have, therefore, laid the foundation for extending investigations to supported catalysts at atmospheric pressure.

To obtain surface information at high pressures, infrared spectroscopy is often employed. It is especially valuable since it can yield both structural and quantitative information. Eischens and co-workers (*17, 18*) were the first to examine the adsorption of CO on supported catalysts with infrared spectroscopy. A portion of the vast infrared literature concerning CO adsorbed on metals and supported catalysts has recently been reviewed by Sheppard and Nguyen (*19*). Baddour and co-workers have combined infrared spectroscopy with reaction rate measurements to simultaneously obtain relative CO surface coverage and oxidation rates with supported Pd (*20*) and Pt (*21*) catalysts. The poor sensitivity of dispersive infrared spectroscopy, however, limited the range of CO coverages that could be followed.

Fourier transform infrared spectroscopy (FT-IR) is significantly more sensitive than dispersive infrared spectroscopy due to its multiplex and optical throughput advantages (*22*). It therefore allows much greater variations in CO surface coverages to be followed. In this study, FT-IR is used to investigate the oxidation of CO on an alumina-supported platinum catalyst. Simultaneous CO coverage and reaction rate measurements have been followed over nearly a 100-fold range of surface coverage. However, absorption by the support prevents the observation of adsorbed oxygen or the Pt-C vibrations which occur below the absorption cut off of the support (*23, 24*). Nevertheless, the use of FT-IR coupled with simultaneous reaction rate measurements can increase the understanding of the catalytic oxidation of CO on supported catalysts under high-pressure operating conditions.

METHODS

The catalyst used in this work was a commercially available 1% platinum on a γ-alumina support with a total surface area of 95 m^2/g (Alpha Products). Transmission electron microscopy (TEM) of the fresh catalyst showed that the Pt particle size was ~40 Å. After cleaning and reaction rate measurements, the Pt particle size increased to ~50 Å. The resolution of the TEM (10 Å) was sufficient to show that the particle size distribution was very narrow. The particles were all within ~20% of the size reported. An alumina support was studied simultaneously in order to determine support effects. It was prepared from Degussa Alon C γ-alumina with a BET surface area of 110 m^2/g. Wafers of each material were formed by pressing ~50 mg of the powders as described previously (*25*). The resulting sample disks were 13 mm in diameter and ~250 μm thick. Both samples were placed in a quartz holder within the infrared cell which was part of a recirculating-flow reactor. The infrared cell was constructed of quartz with KBr windows cemented on both ends. In order to accurately monitor gas-phase concentrations, the optical pathlength of the cell was 10 cm. A nichrome wire heater was wrapped around the cell beneath a layer of insulation. Two thermocouples (0.1 mm diameter chromel–alumel) were placed in the cell. One was pressed against the catalyst sample to monitor its temperature under reactive conditions. The other was placed ~5 mm from the Pt catalyst to monitor the gas-phase temperature. The furnace temperature was controlled using the thermocouple attached to the catalyst. The results presented in this study are for steady-state isothermal catalyst conditions at 460, 490, and 520 K. The exothermicity of the reaction resulted in the temperature of the catalyst being measurably higher than that of the gas phase dur-

ing reaction. Since the furnace was controlled by the catalyst temperature, only the gas-phase temperature varied. Under the most adverse conditions, at the highest temperature and reaction rate, the temperature of the gas was never more than 40 K less than the catalyst temperature.

The entire catalyst cell was mounted on a computer-controlled lateral positioner with 1 μm spatial resolution and a total travel in one direction of 50 mm. Movement of the cell allowed spectra to be obtained alternately of the gas phase, catalyst, or support. The 1 μm precision of the positioner allowed accurate spectral subtractions to be obtained due to the precise repositioning of the samples.

The infrared cell was connected to a bellows-type gas pump and gas inlet apparatus by means of flexible stainless-steel hoses to allow free motion of the cell. The bellows pump was operated at its maximum recycle flow rate of 6 liters/min. The reactant gases were blended in rotometer flow tubes before being introduced into the recirculating flow system. The gases used during oxidation rate studies were certified mixtures of 5% O_2 in nitrogen and 10% CO in nitrogen. Twenty-one percent O_2 in nitrogen and 99.99% CO were used during catalyst cleaning operation discussed below. Early experiments were performed without a metal carbonyl trap on the CO gases. Later a carbonyl trap was added with no appreciable change in the results. Nitrogen at an initial purity of >99.998% was passed through a gas purifier to reduce H_2O and O_2 impurities to $\leq$0.1 ppm during CO desorption experiments. Under reaction conditions, the input flows were always <15% of the recycle flow rate to approximate gradientless reactor conditions (<3% conversion/pass). The total exit flow was measured to $\pm$2% by timing the volume of gas passing through a dry test gas volume meter. During the CO oxidation rate experiments, the 5% O_2 in N_2 flow was kept constant while the flow of 10% CO in N_2 was varied. The resultant concentration of CO, O_2, and CO_2 in the reactor varied from 10^{-8} to 10^{-6} g mole/cm^3 with typical values of 5×10^{-7} g mole CO/cm^3, 5×10^{-7} g mole O_2/cm^3, and 2×10^{-7} g mole CO_2/cm^3 at the maximum in rate of 2.3×10^6 g mole CO/sec observed at 490 K. The rate data are reported as reaction probability (dimensionless) where the turnover number was divided by the CO incidence rate.

Because the maximum temperature of the cell (575 K) was insufficient for obtaining a spectroscopically clean catalyst, reactive cleaning of the catalyst was employed. A stoichiometric excess of carbon monoxide was mixed with 21% O_2 in N_2 while the catalyst cell was held at 550 K. The exothermic oxidation reaction occurring on the catalyst surface resulted in measured catalyst temperatures of 925 K. The combined high temperature and reactive environment served to clean the catalyst as discussed later.

Infrared spectra were obtained with a Nicolet 7199 FT-IR spectrometer. A special high-throughput optical bench, described previously (*25*), was used to improve sensitivity for the low transmission catalyst samples. The spectrometer was purged with dry nitrogen to eliminate interference from CO_2 in the spectrometer atmosphere. Infrared spectra were obtained at 4 cm^{-1} resolution with 200 interferograms averaged. To obtain the infrared spectra of surface species under reaction conditions, spectra of the clean catalyst and gas phase at the reaction temperature were each separately subtracted from the spectra of the catalyst during reaction.

Infrared spectra measured through the catalyst under steady-state reaction conditions provided information to simultaneously measure CO surface coverage and CO oxidation rate. If gradientless conditions are assumed, then the steady-state CO oxidation rate can be calculated from the measured CO and CO_2 concentrations in the reactor, the known concentrations of the gases before mixing, the stoichiometry of the CO oxidation reaction, and the mea-

sured flow of gases exiting the reactor. The gas-phase CO and CO_2 concentrations in the reactor are readily determined from the strength of their infrared absorptions. Because the absorptions of these gases do not follow Beer's law at 4 cm^{-1} resolution, calibration curves of infrared absorption vs concentration were derived from gas mixtures calibrated by gas chromatographic methods.

Reaction rates were measured in the cell without the Pt/Al_2O_3 sample. These experiments showed that reaction occurring in the absence of the catalyst was always less than 2% of the reaction rate measured with the catalyst under identical conditions.

RESULTS

The infrared spectrum of the Pt/Al_2O_3 catalyst is shown before, during, and after the high temperature reactive cleaning in Fig. 1. Before cleaning, the spectral features include a broad structured band above 3000 cm^{-1} due to free OH groups (>3600 cm^{-1}) and hydrogen-bonded OH groups (<3600 cm^{-1}) present on the Al_2O_3 support (Fig. 1A). Hydrocarbon impurity bands appear between 2800 and 3000 cm^{-1}. Carbon dioxide permanently trapped within closed pores of the alumina support has a strong absorption at 2343 cm^{-1} (*26, 27*). The region between 1700 and 1200 cm^{-1} included carbon–oxygen impurities such as carbonates, formates, and bicarbonates on the Al_2O_3 surface. Below 1100 cm^{-1} absorption by the Al_2O_3 support becomes appreciable and spectral information below 1025 cm^{-1} cannot be measured. Figure 1B shows that during the high-temperature reactive cleaning (catalyst temperature measured at 925 K in a stoichiometric excess of CO) all hydrocarbon impurities are removed along with hydrogen-bonded OH groups and most of the carbon–oxygen impurities. Only a small amount of free OH groups remain along with the trapped CO_2 which is distorted by the poor subtraction of the highly absorbing gas phase CO_2. Following the cleaning procedure, H_2O impurities ($\leq$0.1 ppm) in the flowing N_2 gradually replace much of the OH on the alumina surface, but Fig. 1C shows that the catalyst remains relatively free of other contaminants.

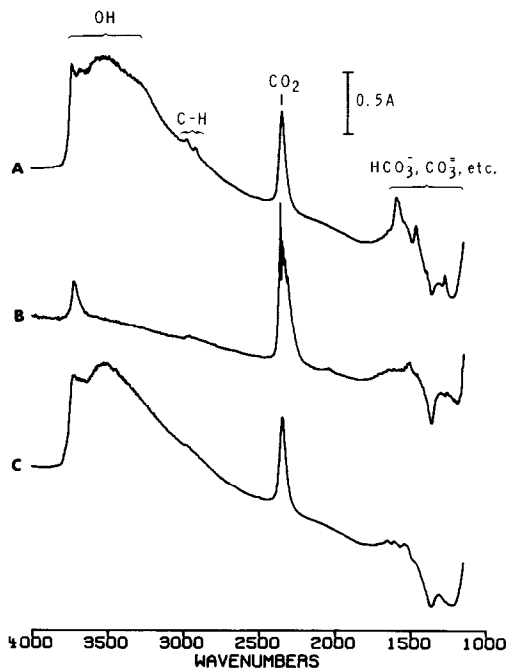

FIG. 1. Spectra of Pt/Al_2O_3 catalyst (A) before cleaning at 550 K, (B) during cleaning in high temperature 925 K reactive CO and O_2 environment (gas phase spectra subtracted), (C) after cleaning at 550 K. The vertical bar indicates scale in absorbance units.

The complete absence of hydrogen-bonded OH during reactive cleaning is noteworthy since even temperatures exceeding 1150 K in vacuum do not eliminate all hydrogen-bonded OH from Al_2O_3 (*28*). It is quite possible that reaction between CO and OH on the alumina occurs at this elevated temperature on Pt/Al_2O_3 as has been proposed previously by Foger and Anderson (*29*). The OH groups on the separate Al_2O_3 sample are only slightly removed although the temperature of this sample which does not promote the CO oxidation remains at ~550 K. It is also possible that the Pt/Al_2O_3 surface temperature exceeds the 925 K temperature measured by the thermocouple. The high-temperature reactive cleaning of the catalyst does result in a

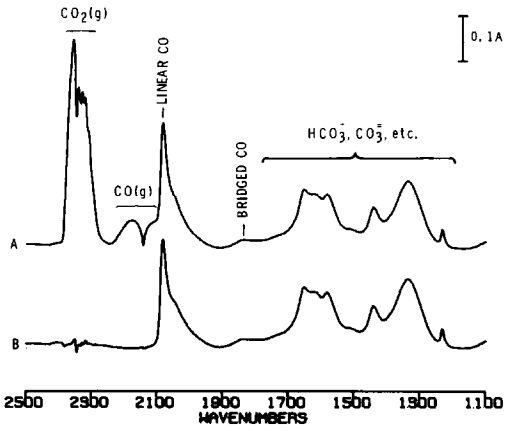

FIG. 2. Spectrum of catalyst during steady-state CO oxidation reaction at 520 K (A) after spectrum of clean catalyst subtracted, (B) further subtraction of gas phase.

partial sintering of the Pt catalyst as evidenced by a ~20% decrease in the maximum intensity of the infrared bands associated with CO adsorbed on Pt. A simultaneous small increase (~3 cm^{-1}) in the infrared frequency of the linearly bound CO also suggests sintering of the Pt as discussed by Solomennikov *et al.* (*30*). Transmission electron microscopy of the catalyst showed an increase of the average Pt particle size to ~50 Å after cleaning.

Figure 2A shows the spectrum of the catalyst during steady-state oxidation of CO at 520 K after the spectrum of the clean catalyst has been digitally subtracted. Gas-phase CO and CO_2 are observed along with chemisorbed CO and carbon–oxygen species generated on the Al_2O_3 during the reaction. Further subtraction of the gas-phase spectra results in the spectrum presented in Fig. 2B. In agreement with traditional assignments (*19*), the peak centered at 2080 cm^{-1} has been assigned to CO linearly bound to the Pt metal surface while the broad, low-intensity peak centered at 1840 cm^{-1} has been assigned to bridge-bonded CO.

The 2035 cm^{-1} shoulder on the low energy side of the 2080 cm^{-1} band is not a result of band distortion due to scattering (i.e., Christiansen effect) since other bands are not similarly distorted and this shoulder is not present at very low CO coverages as discussed later. The assignment of this shoulder is somewhat ambiguous, but it may be a result of CO adsorbed on low coordination Pt sites. The low coordination Pt sites are expected to result in a lower C–O stretching frequency as discussed by van Hardeveld and Hartog (*31*).

The bands below 1700 cm^{-1} are dependent on temperature and gas-phase concentrations. Their frequencies correspond to carbonates, bicarbonates, and formates adsorbed on the Al_2O_3 support. Although there are some questions in the literature as to specific assignments, the peaks in this region have all been observed previously for species adsorbed on Al_2O_3 after exposure to CO or CO_2 (*32–41*).

The steady-state CO oxidation rate data for the catalyst controlled at 460 K are presented in Fig. 3 where the CO reaction probability (dimensionless) is plotted as a function of the ratio of mole fractions of the reactant gas concentrations within the reactor. The reaction probability is plotted rather than the directly measured total rate since this accounts for the changing CO flux to the surface. By plotting the reaction probability vs the ratio of reactant concentrations in the reactor, provision is made for the fact that the partial pressure of neither reactant is held constant within the reactor during reaction for the series of isothermal steady-state experiments. In addition, the hysteresis is made more apparent and the reactant ratio is the suggested link between high- and low-pressure studies (*1*).

The linear-bonded CO infrared peak height, which was measured simultaneously with the 460 K steady-state CO reaction probabilities, is also presented in Fig. 3. A very pronounced hysteresis in both the reaction probability and CO infrared peak height is observed in the data in Fig. 3. Hysteresis effects have been observed previously for the catalytic oxidation of CO and some of the results have

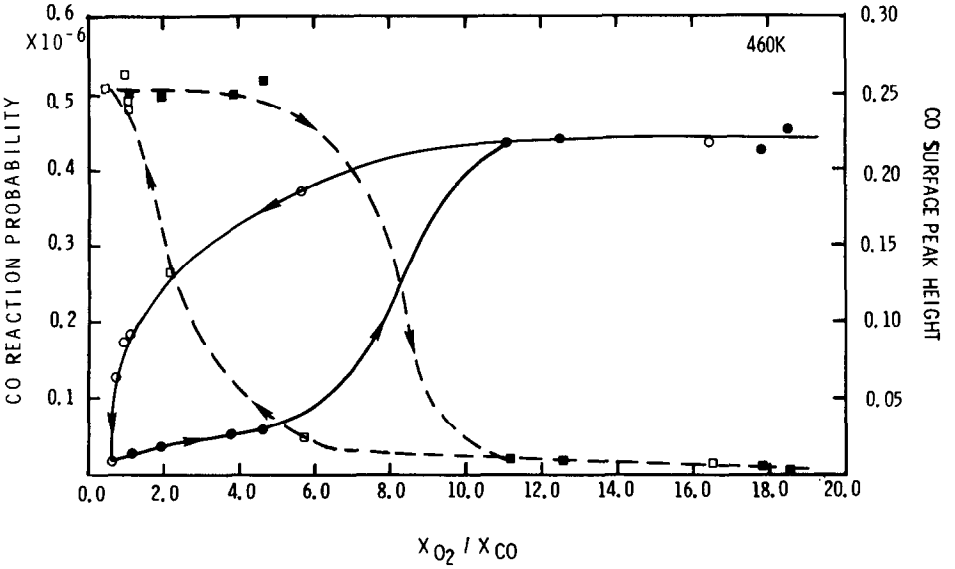

FIG. 3. Steady-state CO oxidation probability and infrared peak height of linear-bound CO (in absorbance units) at 460 K as a function of the relative reactant concentrations in the reactor. Solid line with circles represents reaction probability while dashed line with squares represents CO peak height. Open symbols represent data taken with CO increasing and filled symbols represent data taken with CO decreasing.

been reviewed by Hlavacek and Votruba (*42*). As CO is initially added to oxygen in the reactor, the CO reaction probability remains fairly constant. When the CO concentration approaches stoichiometry the reaction probability drops sharply. In this region of rapidly decreasing CO reaction probability, periodic oscillations in reaction rate, catalyst surface temperature, and CO surface coverage are observed. This is the region where the model calculations of Herz and Marin (*13*) predict multiple rate solutions to occur. These results will be discussed in more detail in a later publication. The reaction probability is nearly quenched (<5% of the maximum) around the stoichiometric point (i.e., $X_{O_2}/X_{CO} = 0.5$). There is, however, measurable reaction still occurring on the catalyst indicating that the reaction is not fully quenched. After the catalyst has been exposed to sufficient CO to retard the rate, a reduction in CO concentration does not yield the expected rapid increase in CO reaction probability. Instead, the CO reaction probability remains low until an additional small decrease in the input CO causes the reaction to suddenly ignite. The result is a rapid temperature rise of the catalyst wafer (≤ 100 K) which persists only briefly as the temperature controller brings the catalyst temperature back to the set point. The ignition of the reaction results in data which are widely separated on the abscissa even though there has been only a small change in the input CO concentration. The lower branch of the rate loop is stable and reversible as long as the reactant concentrations remain below the ignition point.

The hysteresis in the CO infrared peak intensity in Fig. 3 inversely parallels the hysteresis in reaction probability. Integrated intensities and peak heights yield similar results, but integrated intensities tended to be less precise due to their greater dependence on baseline corrections. Additional rate and CO surface-coverage hysteresis loops were obtained at higher tempera-

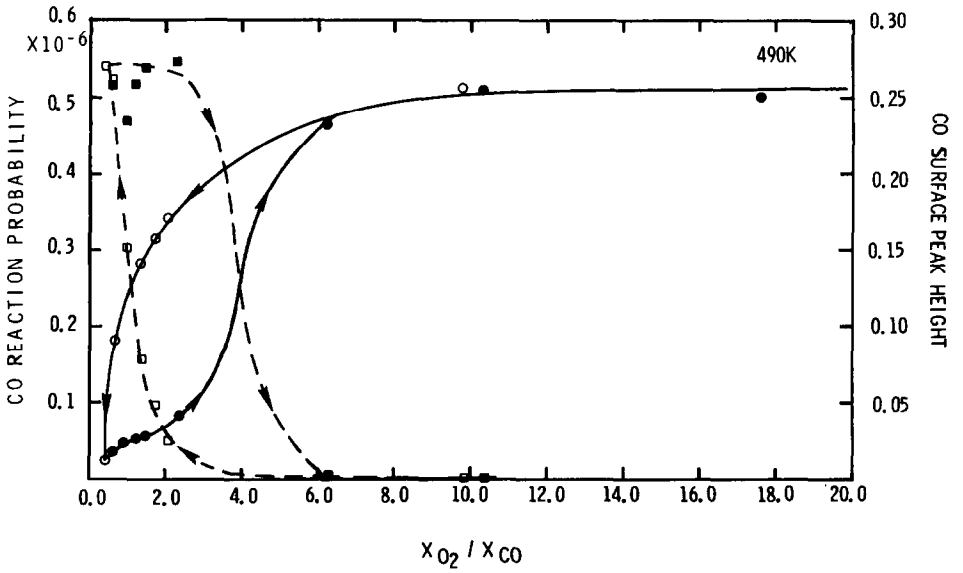

FIG. 4. Steady-state CO oxidation probability and infrared peak height of linear-bound CO (in absorbance units) at 490 K as a function of the relative reactant concentrations in the reactor. Solid line with circles represents reaction probability while dashed line with squares represents CO peak height. Open symbols, CO increasing; filled symbols, CO decreasing.

tures. Figure 4 illustrates steady-state data obtained at 490 K while Figs. 5 and 6 present data acquired at 520 K. Note that the widths of the hysteresis loops decrease with increasing temperature for both the reaction probability and infrared peak height of adsorbed CO. At 520 K the hysteresis loop has almost completely collapsed although there is still a very definite ignition of the reaction which results in a brief 100 K increase in the catalyst temperature. The features of the reaction probability and CO surface coverage continue to parallel each other at each temperature illustrating that the reaction probability and CO surface coverage are intimately linked.

Other trends noted in Figs. 3–6 are that both the extinction of the reaction and the corresponding increase of surface CO have steeper slopes as the temperature is raised. In addition the CO surface concentration is lower at the higher temperatures for a corresponding X_{O_2}/X_{CO} until the rapid increase in surface coverage is reached. It is important to note that the maximum linear-bonded CO coverage obtained at the two lower temperatures under reaction conditions corresponds to the saturation CO coverage obtained when only pure CO is added to the reactor at atmospheric pressure. At 520 K the saturation CO coverage is 20% higher than the maximum CO coverage under steady-state oxidation conditions.

The complex form of the coverage dependence of the rate is shown in Fig. 7 which is a plot of the CO reaction probability as a function of the linear-bonded CO infrared absorption intensity for the 520 K data presented in Figs. 5 and 6. Qualitatively similar plots are obtained at the lower temperatures. The catalytic activity is markedly poisoned by the chemisorbed CO. However, it is surprising to note that the CO reaction probability can still be at a moderate level when the CO surface coverage reaches its maximum value under reaction conditions. A small increase in the CO inlet concentration at this point results in a sharp

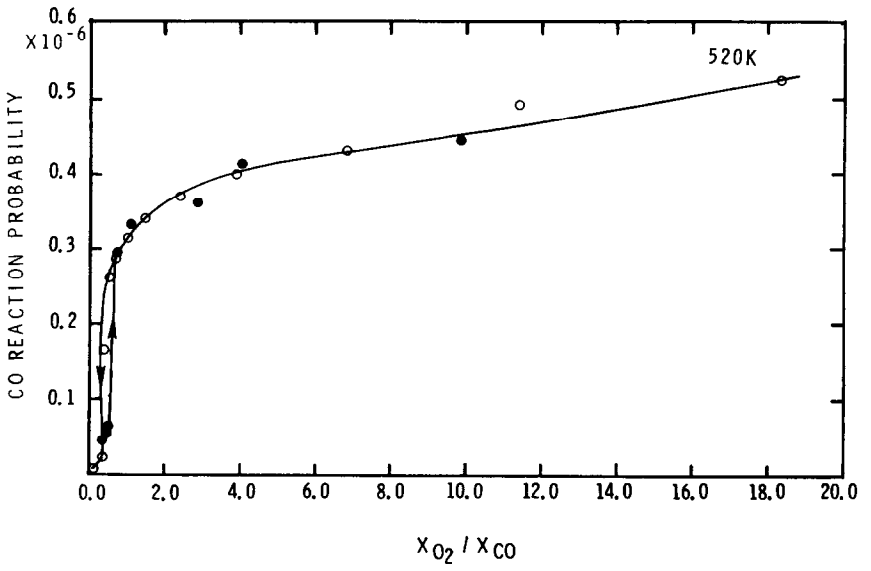

FIG. 5. Steady-state specific CO oxidation reaction rate at 520 K as a function of the relative reactant concentrations in the reactor. ○, increasing CO; ●, decreasing CO.

reduction of the reaction with no increase in the CO surface coverage. A careful examination of both the linear and bridge-bonded CO shows that neither infrared absorptions increase in intensity during this final extinction of the reaction. In fact, occasionally there is even a slight decrease in the intensity of these bands during the final rate extinction. At the same time that the rapid drop in reaction rate occurs, the bands due

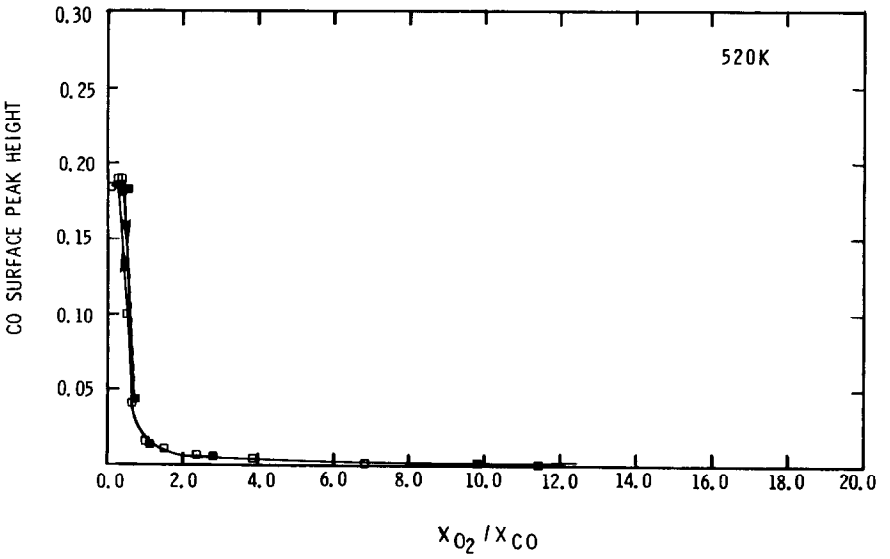

FIG. 6. Peak height in absorbance units of CO linearly bound to Pt during steady-state oxidation at 520 K as a function of the relative reactant concentrations in the reactor. □, increasing CO; ■, decreasing CO.

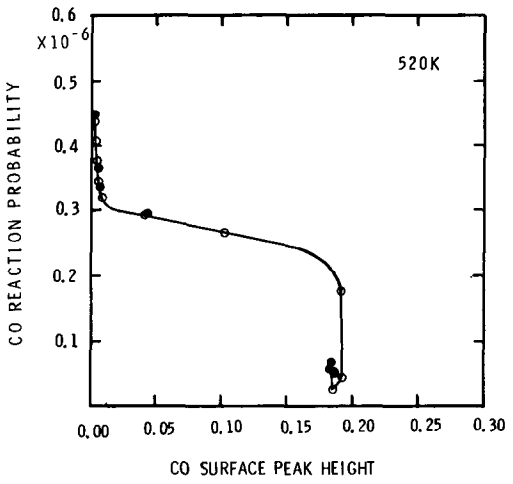

FIG. 7. Steady-state data at 520 K from Figs. 5 and 6. ○, increasing CO; ●, decreasing CO.

to the carbonates, bicarbonates, and formates on the Al_2O_3 support decrease in intensity. This latter observation is most likely a result of the low rate of reaction and the drop in gas phase CO_2 concentration.

In addition to the infrared band intensities, the peak positions for the linear and bridge-bonded CO were followed under reactive and nonreactive conditions. The frequency of the linear-bonded CO infrared peak was found to be invariant during the oxidation reaction even though the peak intensities could be followed over changes of almost two orders of magnitude. Figure 8 shows the linear-bound CO infrared band at maximum coverage during oxidation at 520 K and at intermediate coverages representing approximately 50 and 5% of the maximum coverage. The peak position is invariant at 2081 cm^{-1} over this coverage range. Lower coverages (<5%) result in a 1–3 cm^{-1} increase in frequency at the three temperatures studied. There is a slight increase in the energy of the linear-bound CO stretching vibration as the temperature is lowered. Thus the position at maximum coverage at 490 K is 2082 cm^{-1} and 2084 cm^{-1} at 460 K. At each temperature, the CO stretching frequency under reactive conditions are found to be within 1 cm^{-1} of the frequency when the catalyst is exposed to 100% CO at atmospheric pressure.

These results are in sharp contrast to the changes in peak position observed for the same band during nonreactive desorption of CO into flowing N_2 at the same catalyst temperatures. Figure 9 illustrates this point at 520 K. The initial CO coverage was obtained by exposing the catalyst to 10% CO in N_2 at one atmosphere. A 34 cm^{-1} decrease in the energy of the linear-bound CO vibration results from the same 20-fold change in peak intensity shown in Fig. 8. During the desorption experiments, the peak intensity and frequency shift of both the linear and bridge-bonded CO are functions of temperature, pretreatment, initial CO gas-phase concentration, and the presence of trace impurities of O_2. In addition, steady-state isothermal adsorption experiments involving 1 and 10% mixtures of CO in N_2 show shifts to lower energy of 3–5 cm^{-1} in the C–O stretching frequency relative to that found for adsorbed CO in 100% CO at atmospheric pressure. The details of

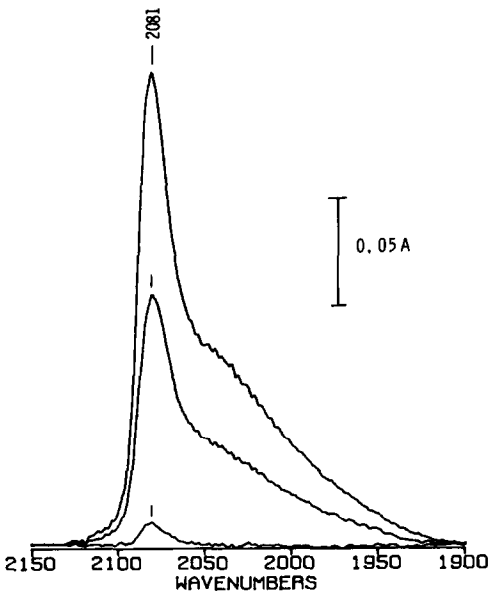

FIG. 8. Difference spectra of linear-bonded CO at different steady-state coverages during oxidation at 520 K.

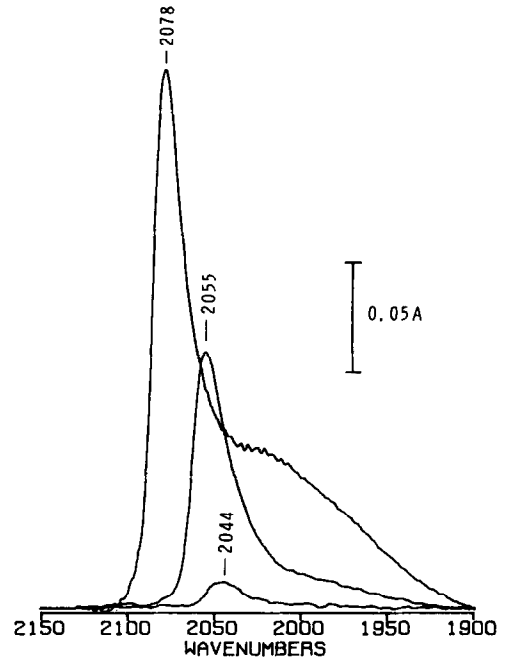

FIG. 9. Difference spectra of linear-bonded CO at different coverages during thermal desorption into flowing N_2 at 520 K.

a variety of CO thermal desorption experiments will be the subject of a later paper (*43*). The important point to note, however, is the very different results for CO chemisorption observed during reactive and nonreactive conditions.

Because of the broad, low-intensity nature of the bridge-bonded CO as well as sloping baselines in that region, it was only possible to follow the absorption of bridge-bonded CO over a factor of three variation in intensity. Within that limit, the bridge-bonded CO does not appear to vary in peak position. Furthermore, under reaction conditions, the ratio of intensities of linear and bridge-bonded CO is found to be invariant. These points are illustrated in Fig. 10 where 50% coverage and 100% coverage are compared for steady state at 520 K. In Fig. 10, the absorption at 50% coverage has been scale expanded such that the linear-bonded CO peak intensities coincide. It is clear from Fig. 10 that the bridge and linear-bonded CO coverages change at the same rate. It is also apparent from Fig. 10 that the shoulder on the 2081 cm^{-1} peak scales with the 2081 cm^{-1} peak for moderate to high surface coverage. However, at surface coverages $\leq 5\%$, the low frequency shoulder is not present as exhibited in Fig. 11. The 5% coverage 2081 cm^{-1} peak at 520 K steady-state oxidation conditions has been scale expanded in Fig. 11 to the same intensity as the maximum coverage peak. The absence of the low-energy shoulder at low CO coverage is readily apparent. A similar absence of a low-energy shoulder at low CO coverages is found under nonreactive desorption conditions.

DISCUSSION

The most striking result of this study is the invariance of the peak position of the linear-bonded CO over almost 2 orders of magnitude change in peak intensity during the catalytic oxidation of CO on Pt/Al_2O_3.

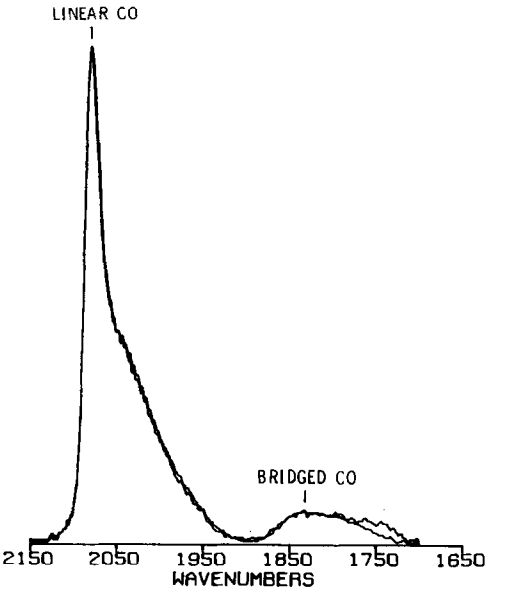

FIG. 10. Difference spectra of linear and bridge-bonded CO at full and half coverage during steady-state reaction at 520 K. Half coverage spectra scale expanded such that intensities of linear-bonded CO coincide for both coverages.

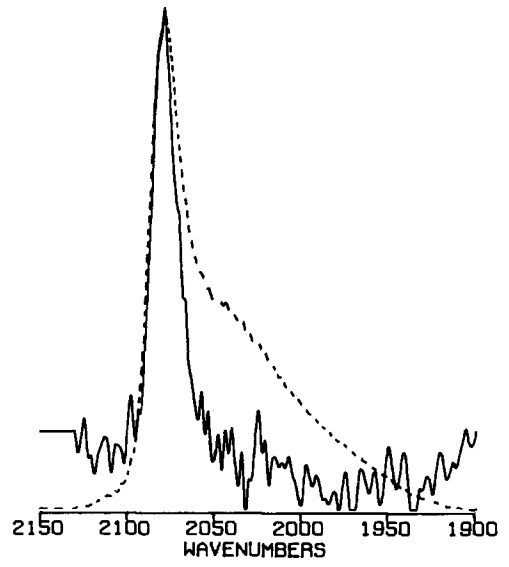

FIG. 11. Maximum coverage and 5% coverage of linear-bonded CO during steady-state oxidation at 520 K. (----) Maximum coverage, (———) 5% coverage scale expanded to same intensity as maximum coverage peak.

In addition, at each temperature this invariant C–O stretching frequency during oxidation is within 1 cm^{-1} of the value obtained under nonreactive conditions in 100% CO at atmospheric pressure. The relative amounts of linear and bridge-bonded CO are also constant with changes in total CO surface coverage over the range studied. These results are in sharp contrast to the large changes in peak position observed with coverage during nonreactive thermal desorption from the same catalyst. The large shifts in infrared CO peak position with surface coverage under nonreactive conditions have been observed before on supported catalysts (*18, 44*) but have been more extensively studied on ribbons or single crystals of Pt, Pd, Ru, Cu, or Ir (*45–51*). Studies with isotopic mixtures of CO clearly demonstrate that coupling between the adsorbed molecules is responsible for the frequency shift. The coupling has been explained as resulting from dipole–dipole coupling, vibrational coupling arising from through-metal interactions, coverage-dependent metal-adsorbate bond strength due to a modification of the local field acting on the adsorbate, direct intermolecular repulsion, or a combination of several of the above (*45–54*). Recently, comparison of frequency shifts predicted from theoretical calculations with the experimentally measured shifts has suggested that dipole–dipole interactions can adequately account for the infrared frequency shifts observed on Pt (*46, 54*). However, it is apparent that other adsorbate molecules (e.g., hydrocarbons, H_2O, oxygen, etc.) can modify the backbonding of the Pt *d* electrons to the 2 π^* level in the adsorbed CO and cause a shift in frequency of the observed CO stretching vibration (*55*).

Nevertheless, the invariance of the CO infrared band position under reaction conditions indicates that either the environment of each chemisorbed CO molecule is constant over a large range of CO surface coverages or the expected change in C–O stretching frequency is eliminated or compensated by other environmental effects. Co-adsorbed oxygen is known to increase the C–O stretching frequency (*56*) and, therefore, could compensate for decreases in frequency with diminishing CO surface coverage. However, the absence of frequency shifts over the very large range of CO surface coverages studied would seem to reasonably eliminate an exact compensation by oxygen coadsorption. In addition, the high-resolution electron energy loss spectroscopy studies by Thomas and Weinberg (*56*) involving coadsorbed CO and O on Ru(001) show that the C–O stretching frequency shifts with coverage even in the presence of fixed or changing oxygen coverage. Thus the presence of coadsorbed oxygen cannot reasonably account for the invarient infrared CO frequency during oxidation.

Therefore, during oxidation the local CO environment of each chemisorbed molecule is constant over nearly two orders of magnitude change in surface coverage. This local environment must also be equivalent to that

of saturated CO coverage since the infrared peak positions and relative linear to bridge-bonded CO coverages are the same as found with CO adsorbed on the catalyst in the presence of 100% CO at atmospheric pressure. These observations can be accounted for by two possibilities: (i) the formation of domains or "islands" of CO occurs on the Pt surface during oxidation or (ii) mass diffusion limitations cause internal concentration gradients such that a saturated layer of adsorbed CO forms on the outer surface of the catalyst wafer combined with a sharp drop in CO surface coverage inside this outer layer. The latter scenario requires a near step function dependence of CO surface coverage with CO partial pressure. In the first case, changes in infrared peak heights result from changes in the size and/or number of CO islands while in the latter case, changes in peak height reflect changes in the thickness of the region of the saturated CO coverage within the wafer.

Both experimental evidence and mass diffusion calculations eliminate the second explanation and, therefore, confirm the formation of CO islands during catalytic CO oxidation. Mass diffusion limitations were ruled out by performing the classical Koros–Nowak experiment (*57*). For a 10-fold change in Pt dispersion, the rates per Pt site were within experimental error. Furthermore, the concentration profile within the disk was calculated using the CO concentration-sensitive reaction rate model proposed by Herz and Marin (*13*). The measured value of the effective diffusivity (0.02 cm^2/sec) was used with the constraint that the calculated flux at the surface of the disk match the observed rate. Under our conditions, the calculated CO surface coverage did not change throughout the disk.

Further evidence against a diffusion induced saturated CO region at the edge of the disk lies in the infrared spectra. The change in shape of the infrared band with CO coverage in Fig. 11 cannot be explained by a change in the thickness of a saturated layer of CO. The change in the shoulder observed in Fig. 11 may be due to changes in adsorption of low-coordination sites with the CO islands initially forming on the low-index crystallite faces. In addition, the C–O stretching frequencies cannot be explained in terms of a diffusion-induced saturated CO region layer. There is a 3–5 cm^{-1} shift to higher frequencies and an increase in band intensity when the gas-phase CO concentration is changed from 1 to 100% CO under nonreactive conditions. At the maximum rate of oxidation in these studies, the CO concentration is ~1%, yet the CO infrared peak position is within 1 cm^{-1} of that found with 100% CO in the absence of oxygen. A CO adsorption region layer caused by diffusional limitations during reaction with a steady-state CO concentration of ~1% would be expected to have a CO infrared frequency 3–5 cm^{-1} lower than actually observed. The evidence for CO island formation is therefore quite compelling.

The studies of Crossley and King (*46, 47*) involving CO adsorption on single crystal Pt suggest that a shift of the CO stretching vibration to lower frequencies should be observed as the CO island size becomes very small since perimeter CO molecules become a significant portion of the island. Based on the 50 Å Pt particle size used in this experiment, it might then be expected that a shift to lower energies should eventually occur over the nearly 2 orders of magnitude change in CO coverage observed in this study. However, an increase in vibrational energy of 1 to 3 cm^{-1} is observed at each temperature as the CO coverage drops below 2–5% of the maximum coverage during oxidation. In our investigation, this observation could be attributed to the influence of coadsorbed oxygen which was not present in the studies of Crossley and King.

The formation of islands of CO and possibly oxygen has recently been suggested from the interpretation of experiments involving metal films or single crystals in the presence of both CO and O_2 at very low pressures ($<10^{-2}$ Pa) (*3, 9, 10, 15, 16*) or

when CO and O_2 are coadsorbed on these metals under UHV conditions (*1, 5*). Ivanov *et al.* (*3*) suggested that the very small preexponential factor for CO_2 formation in their CO oxidation studies at very low pressures on Ir might be a result of separate islands of adsorbed CO and O. More recently, Matsushima (*9*) found that kinetic data from ^{13}C tracer experiments involving the CO oxidation over Pt could be explained in terms of adsorbed CO islands. Coadsorption of oxygen and CO on single crystal metal surfaces has been studied by Ertl and co-workers (*1, 5*) using LEED techniques. They find that during coadsorption both CO_{ad} and O_{ad} form domains. Reflection–adsorption infrared studies have been carried out on Pt (*15*) and Ir (*16*) ribbons which were covered with adsorbed CO and then allowed to react with oxygen. Since infrared CO band positions were found to be nearly invariant, the authors concluded that large CO domains were formed under their reaction conditions near room temperature at low pressures. Our studies extend these recent findings for CO island formation to Pt surfaces of a commercial, high surface area Pt/Al_2O_3 catalyst under steady-state reaction conditions at a total pressure of one atmosphere. In addition, it was possible in this study to monitor both linear and bridge-bonded CO surface coverages during the oxidation of CO. During the revision of this manuscript, Cant and Donaldson (*58*) reported infrared studies of CO oxidation on Pt/SiO_2. They report CO island formation in a dynamic reaction system which is in agreement with our steady-state results.

The existence of CO islands during reaction has important implications in the use of infrared spectroscopy to measure CO surface coverage. In the absence of oxygen, relative surface coverage cannot be obtained from ir measurements alone since the changing dipole–dipole coupling with coverage results in a change in the absorption coefficient per CO molecule. However, under reaction conditions where the peak position is invariant (i.e., relatively large CO islands and constant dipole–dipole coupling), the band intensity should be an accurate measure of relative CO surface coverages. This feature of island formation simplifies the interpretation of the simultaneous reaction rate and CO absorption data obtained by ir spectroscopy. Thus, the CO peak intensity plots in Figs. 3, 4, and 6 represent relative CO surface coverages as a function of reactant concentrations.

The presence of islands also has some important implications regarding the possible kinetic steps occurring on the Pt surface. The presence of CO islands suggests that either the reaction of CO and adsorbed oxygen occurs at the perimeter of the islands or the reaction proceeds by CO species not readily observed by infrared. Because adsorbed CO is more mobile than adsorbed oxygen on the Pt surface at the temperatures used in this study (*1*), the second possibility seems more reasonable. This latter possibility would suggest that CO from the gas phase could react with adsorbed oxygen or more likely that the steady-state concentration of reactive adsorbed CO was at a very low concentration. The reactive CO could be isolated adsorbed CO molecules formed upon initial adsorption on an isolated Pt site or formed by breaking away from the perimeter of the islands. Under these conditions, the infrared CO intensities would only be due to those inactive species adsorbed on the surface, and the infrared intensities would serve only to provide information about that portion of the Pt surface unavailable for reaction.

The inverse relationship between CO surface coverage and reaction probability (Figs. 3–6) is easily explained in terms of a classical site blocking or "poisoning" of the Pt by the adsorbed CO. The branching which leads to the hysteresis loop is generated when the catalyst becomes saturated with CO on the surface. The high surface coverage of CO aids the extinction of the reaction. The necessity of removing some of the adsorbed CO before the reaction can

ignite results in the rate remaining low and therefore the observed hysteresis. The decrease in the size of the hysteresis loop with increasing temperature can be qualitatively understood as resulting from the greater rate of desorption of CO at higher temperatures. Thus the onset of reaction ignition can occur when there is more CO in the gas phase at higher temperatures. This is reasonable because there is a greater rate of desorption of CO as the temperature is raised from 460 to 520 K. This is observed in our experiments involving CO desorption into flowing N_2 (*43*), and it has been found previously that the thermal desorption of CO from Pt surfaces is rapidly changing in this temperature range (*59, 60*).

The high oxidation rates of the upper branch of the hysteresis loop are maintained because the surface coverage of CO is kept low by the ongoing reaction. As the CO partial pressure is increased, the rate of CO adsorption is increased, and the resulting formation of larger islands of CO eventually reduces the reaction rate. The onset of the extinction and the rate of change of CO surface coverage are steeper at higher temperatures because the increased rate of CO desorption must be overcome by a higher CO partial pressure to increase the net rate of CO adsorption. Therefore, the general features of the hysteresis loops presented in Figs. 3–6 can be explained in terms of Pt site blocking by CO and changes in the rate of CO desorption with temperature.

However, adsorbed CO does not appear to be the only factor influencing the extinction of the CO oxidation rate. The plot of reaction probability as a function of CO surface coverage (Fig. 7) clearly shows that both the initial and final drop in reaction probability are not accompanied by significant changes in CO peak height. Neither the linear nor bridge-bonded CO increase during the final precipitous drop in reaction probability. In fact, at times the final drop in reaction probability can be accompanied by a decrease in CO peak intensities (see for example the filled circles in Fig. 7 or the filled squares in Fig. 4). Since no shift in peak position accompanies this change, absorption coefficients should be considered constant and a decrease in intensity will reflect a decrease in CO surface coverage. Thus it is possible that some surface species other than linear or bridge-bonded CO, which has yet to be identified, is responsible for the rapid drops in CO reaction probability. In this case, the surface species responsible for the extinction are either infrared inactive or in a region of the spectrum obscured by the absorption of the Al_2O_3 support or by the absorption of other surface species. The species responsible for the extinction of the reaction cannot, therefore, be directly determined from these experiments. Alternatively, it is possible that the final extinction is associated with the coverage of highly reactive Pt sites which are few in number. Thus, the rapid extinction of the reaction could occur with no noticeable change in the CO surface coverage.

SUMMARY

During oxidation of CO on Pt/Al_2O_3, adsorbed CO is shown to exist in islands on the Pt surfaces. Similar large domains of CO are not found during nonreactive desorption from the same catalyst. Simultaneous monitoring of the rate of reaction and CO surface coverage show that the rate and coverage are coupled. Thus both exhibit pronounced hysteresis loops which are inversely related. The changes in size and shape of the hysteresis loops with temperature are qualitatively understood in terms of the limiting desorption rate of adsorbed CO. However, the reaction probability is not linearly related to the surface coverage of linear or bridge-bonded CO. This would indicate the presence of a yet to be determined surface species or the presence of a very small number of highly reactive Pt sites.

ACKNOWLEDGMENTS

The authors would like to acknowledge the assistance of G. E. Rivord in the construction of the recy-

cle-flow reactor and of F. T. Walder for collection of much of the experimental data. W. R. Sorenson performed the TEM analyses of the catalyst. The Pt/Al_2O_3 catalysts used in Koros–Nowak experiment were kindly donated by Dr. J. L. Gland of General Motors Research Laboratories.

REFERENCES

1. Engel, T., and Ertl, G., *in* "Advances in Catalysis" (D. D. Eley, H. Pines, and P. B. Weisz, Eds.), Vol. 28, p. 1. Academic Press, New York, 1972.
2. Zhdan, P. A., Boreskov, G. K., Egelhoff, W. F., Jr., and Weinberg, W. H., *Surface Sci.* **61,** 377 (1976).
3. Ivanov, V. P., Boreskov, G. K., Shavchenko, V. I., Egelhoff, W. F., Jr., and Weinberg, W. H., *J. Catal.* **48,** 26 (1977).
4. Engel, T., and Ertl, G., *J. Chem. Phys.* **69,** 1267 (1978).
5. Conrad, H., Ertl, G., and Küppers, J., *Surface Sci.* **76,** 323 (1978).
6. Engel, T., and Ertl, G., *Chem. Phys. Lett.* **54,** 95 (1978).
7. Campbell, C. T., Ertl, G., Kuipers, H., and Segner, J., *J. Chem. Phys.* **73,** 5862 (1980).
8. Matsushima, T., *J. Catal.* **55,** 337 (1978).
9. Matsushima, T., *Surface Sci.* **79,** 63 (1979).
10. Matsushima, T., *Surface Sci.* **87,** 665 (1979).
11. Monroe, D. R., and Merrill, R. P., *J. Catal.* **65,** 461 (1980).
12. Fair, J. A., and Madix, R. J., *J. Chem. Phys.* **73,** 3486 (1980).
13. Herz, R. K., and Marin, S. P., *J. Catal.* **65,** 281 (1980).
14. Creighton, J. R., Tseng, F. H., White, J. N., and Turner, J. S., *J. Phys. Chem.* **85,** 703 (1981).
15. Shigeishi, R. A., and King, D. A., *Surface Sci.* **75,** L397 (1978).
16. Reinalda, D., and Ponec, V., *Appl. Surf. Sci.* **5,** 98 (1980).
17. Eischens, R. P., Pliskin, W. A., and Frances, S. A. *J. Chem. Phys.* **22,** 1786 (1954).
18. Eischens, R. P., Francis, S. A., and Pliskin, W. A., *J. Phys. Chem.* **60,** 194 (1956).
19. Sheppard, N., and Nguyen, T. T., *in* "Advances in Infrared and Raman Spectroscopy" (R. J. H. Clark and R. E. Hester, Eds.), Vol. 5, p. 67. Heyden and Son, London, 1978.
20. Baddour, R. F., Modell, M., and Heusser, U. K., *J. Phys. Chem.* **72,** 3621 (1968).
21. Cochran, H. D., Donnelly, R. G., Modell, M., and Baddour, R. F., *Colloid Interface Sci.* **3,** 131 (1976).
22. Griffiths, P. R., "Chemical Infrared Fourier Transform Spectroscopy." Wiley and Sons, New York, 1975.
23. Gland, J. L., Sexton, B. A., and Fisher, G. B., *Surface Sci.* **95,** 587 (1980).
24. Baro, A. M., and Ibach, H., *J. Chem. Phys.* **71,** 4812 (1979).
25. Haaland, D. M., *Surface Sci.* **102,** 405 (1981).
26. Parkyns, N. D., *J. Catal.* **27,** 34 (1972).
27. Peri, J. B., *J. Phys. Chem.* **79,** 1582 (1975).
28. Peri, J. B., *J. Phys. Chem.* **69,** 220 (1965).
29. Foger, K., and Anderson, J. R., *Appl. Surface Sci.* **2,** 335 (1979).
30. Solomennikov, A. A., Lokhov, Y. A., Davydov, A. A., and Ryndin, Y. A., *Kinet. Catal.* **20,** 589 (1979).
31. van Hardeveld, R., and Hartog, F., *in* "Advances in Catalysis" (D. D. Eley, H. Pines, and P. B. Weisz, Eds.), Vol. 22, p. 75. Academic Press, New York, 1972.
32. Little, L. H., and Amberg, C. H., *Canad. J. Chem.* **40,** 1997 (1962).
33. Fink, P., *Z. Chem.* **7,** 324 (1967).
34. Gregg, S. J., and Ramsay, J. D. F., *J. Phys. Chem.* **78,** 1243 (1969).
35. Parkyns, N. D., *J. Chem. Soc. (A)* 1910 (1967) and 410 (1969).
36. Parkyns, N. D., *J. Phys. Chem.* **69,** 211 (1965).
37. Grigor'ev, Y. M., Pozdnyakov, D. V., and Filimonov, V. N., *Russ. J. Phys. Chem.* **46,** 186 (1972).
38. Palazov, A., and Kadinov, G., *Izv. Khim.* **8,** 762 (1975).
39. Rosynek, M. P., *J. Phys. Chem.* **79,** 1280 (1975).
40. Morterra, G., Coluccia, S., Ghiotti, G., and Zecchina, A., *Z. Phys. Chem.* **104,** 275 (1977).
41. King, S. T., *Appl. Spec.* **34,** 632 (1980).
42. Hlavacek, V., and Votruba, J., *Adv. Catal.* **27,** 59 (1978).
43. Haaland, D. M., and Williams, F. L., in preparation.
44. Heyne, H., and Tompkins, F. C., *Trans. Faraday Soc.* **63,** 1274 (1967).
45. Shigeishi, R. A., and King, D. A., *Surface Sci.* **58,** 379 (1976).
46. Crossley, A., and King, D. A., *Surface Sci.* **68,** 528 (1977).
47. Crossley, A., and King, D. A., *Surface Sci.* **95,** 131 (1980).
48. Bradshaw, A. M., and Hoffman, F. M., *Surface Sci.* **72,** 513 (1978).
49. Pfnür, H., Menzel, D., Hoffman, F. M., Ortega, A., and Bradshaw, A. M., *Surface Sci.* **93,** 431 (1980).
50. Reinalda, D., and Ponec, V., *Surface Sci.* **91,** 113 (1979).
51. Hollins, P., and Pritchard, J., *in* "Vibrational Spectroscopies for Adsorbed Species" (A. T. Bell and M. L. Hair, Eds.) ACS Symposium Series, Vol. 137, p. 51. American Chemical Society, Washington, DC, 1980.
52. Mahan, G. D., and Lucas, A. A., *J. Chem. Phys.* **68,** 1344 (1978).
53. Moskovits, M., and Hulse, J. E., *Surface Sci.* **78,** 397 (1978).

54. Scheffler, M., *Surface Sci.* **81,** 562 (1979).
55. Primet, M., Basset, J. M., Mathieu, M. V., and Prettre, M., *J. Catal.* **29,** 213 (1973).
56. Thomas, G. E., and Weinberg, W. H., *J. Chem. Phys.* **70,** 954 (1979).
57. Koros, R. M., and Nowak, E. J., *Chem. Eng. Sci.* **22,** 470 (1967).
58. Cant, N. W., and Donaldson, R. A., *J. Catal.* **71,** 320 (1981).
59. Collins, D. M., and Spicer, W. E., *Surface Sci.* **69,** 85 (1977).
60. Hopster, H., and Ibach, H., *Surface Sci.* **77,** 109 (1978).